THE ASTROPHYSICAL JOURNAL, 505:974–983, 1998 October 1

MAGNETOHYDRODYNAMIC TURBULENCE OF CORONAL ACTIVE REGIONS AND THE DISTRIBUTION OF NANOFLARES

PABLO DMITRUK[1] AND DANIEL O. GÓMEZ[2,3]
Departamento de Física, Facultad de Ciencias Exactas y Naturales, Universidad de Buenos Aires, Ciudad Universitaria, Pabellón I, 1428 Buenos Aires, Argentina; dmitruk@df.uba.ar

AND

EDWARD E. DELUCA
Harvard-Smithsonian Center for Astrophysics, 60 Garden St., Cambridge MA 02138
Received 1997 October 30; accepted 1998 May 4

ABSTRACT

We present results from numerical simulations of an externally driven two-dimensional magnetohydrodynamic system over extended periods of time, used to model the dynamics of a transverse section of a solar coronal loop. A stationary forcing was imposed to model the photospheric motions at the loop footpoints. After several photospheric turnover times, a turbulent stationary regime is reached that has an energy dissipation rate consistent with the heating requirements of coronal loops. The turbulent velocities obtained in our simulations are consistent with those derived from the nonthermal broadening of coronal spectral lines. We also show the development of small scales in the spatial distribution of electric currents, which are responsible for most of the energy dissipation. The energy dissipation rate as a function of time displays an intermittent behavior, in the form of impulsive events, that is a direct consequence of the strong nonlinearity of the system. We associate these impulsive events of magnetic energy dissipation with the so-called nanoflares. A statistical analysis of these events yields a power-law distribution as a function of their energies with a negative slope of 1.5, consistent with those obtained for flare energy distributions reported from X-ray observations. A simple model of dissipative structures, based on Kraichnan's theory for MHD turbulence, is also presented.

Subject headings: MHD — Sun: corona — Sun: flares — turbulence

1. INTRODUCTION

Various scenarios for the heating of coronal loops in active regions have been proposed, most of which have in common the formation and dissipation of highly structured electric currents. The spontaneous formation of tangential discontinuities (Parker 1972, 1983), the development of an energy cascade driven by random footpoint motions on a force-free configuration (van Ballegooijen 1986), or the direct energy cascade associated with a fully turbulent magnetohydrodynamic (MHD) regime (Heyvaerts & Priest 1992; Gómez & Ferro Fontán 1992) are a few examples. The main conclusion is that the formation of small scales in the spatial distribution of electric currents is necessary to enhance magnetic energy dissipation and therefore provide sufficient heating to the plasma confined in these loops.

The dynamics of a coronal loop driven by footpoint motions can be described by MHD equations. Since the kinetic (R) and magnetic (S) Reynolds numbers in coronal active regions are extremely large ($R \sim S \sim 10^{10-12}$), we expect footpoint motions to drive the loop into a strongly turbulent MHD regime. Footpoint motions, whose length scales are usually much smaller than the loop length, will cause the coronal plasma to move in planes perpendicular to the axial magnetic field, generating small transverse components of the magnetic and velocity fields. The nonlinear dynamics of these fields can be adequately described using two-dimensional MHD equations. In this paper we present numerical integrations of these equations, considering the driving action of footpoint motions on a generic transverse section of a loop. In § 2 we model this coupling, and in § 3 we describe the numerical technique used for the integration of the two-dimensional MHD equations. In § 4 we report the energy dissipation rate and turbulent or excess velocity that we obtain, and describe the temporal series of magnetic and kinetic energies. The energy power spectra computed from our simulations are shown in § 5. The spatial structures developed by this system, such as the formation of small scales in the distribution of electric currents, are presented in § 6.

In § 7 we perform a statistical analysis of the dissipation events and study the correlations between different variables. In § 8 we discuss some of the implications of our results. For instance, in § 8.1 we present a simple model for the dissipative structures of a turbulent MHD system, and compare the predictions arising from this model with the results obtained from our simulations. In § 8.2 we discuss the relevance of heating theories for the thermal balance of active regions, which is globally characterized by the scaling laws. Different theories give rise to different relationships between parameters of the active region loops, such as the pressure, temperature, magnetic intensity, and length. The possible connection between the dissipation events studied in this paper and the much larger ones involved in solar flares is discussed in § 8.3. Finally, in § 9 we summarize the main conclusions of this paper.

2. EQUATIONS FOR TWO-DIMENSIONAL MAGNETOHYDRODYNAMICS

The dynamics of a coronal loop with a uniform magnetic field $\boldsymbol{B} = B_0 z$, length L, and transverse section $(2\pi l) \times (2\pi l)$ can be modeled by the reduced magnetohydrodynamic

[1] Fellow of Universidad de Buenos Aires.
[2] Also at the Instituto de Astronomía y Física del Espacio, Buenos Aires, Argentina.
[3] Member of the Carrera del Investigador, Consejo Nacional de Investigaciones Cientificas y Tecnicas (CONICET), Argentina.

(RMHD) equations (Strauss 1976)

$$\partial_t a = v_A \partial_z \psi + [\psi, a] + \eta \nabla^2 a , \quad (1)$$

$$\partial_t w = v_A \partial_z j + [\psi, w] - [a, j] + \nu \nabla^2 w , \quad (2)$$

where $v_A = B_0/(4\pi\rho)^{1/2}$ is the Alfvén speed, ν is the kinematic viscosity, η is the plasma resistivity, ψ is the stream function, and a is the vector potential. The fluid vorticity is $w = -\nabla^2\psi$, $j = -\nabla^2 a$ is the electric current density, and $[u, v] = z \cdot \nabla u \times \nabla v$. For given horizontal photospheric motions applied at the footpoints (plates $z = 0$ and $z = L$), transverse velocity and magnetic field components develop in the interior of the loop, given by $\boldsymbol{v} = \nabla \times (z\psi)$ and $\boldsymbol{b} = \nabla \times (za)$.

The RMHD equations can be regarded as describing a set of two-dimensional MHD systems stacked along the loop axis and interacting among themselves through the $v_A \partial_z$ terms (see, e.g., Hendrix & van Hoven 1996). For simplicity, hereafter we study the evolution of a generic two-dimensional slice of a loop. We therefore model the $v_A \partial_z$ terms given in equations (1)–(2) as external forces. To this end, we assume the vector potential to be independent of z and the stream function to interpolate linearly between $\psi(z = 0) = 0$ and $\psi(z = L) = \Psi$, where $\Psi(x, y, t)$ is the stream function for the photospheric velocity field. These assumptions yield $v_A \partial_z \psi = v_A \Psi/L$ (in eq. [1]) and $v_A \partial_z j = 0$ (in eq. [2]). These approximate expressions correspond to an idealized scenario in which the magnetic stress distributes uniformly throughout the loop. The two-dimensional equations for a generic transverse slice of a loop become

$$\partial_t a = [\psi, a] + \eta \nabla^2 a + f , \quad (3)$$

$$\partial_t w = [\psi, w] - [a, j] + \nu \nabla^2 w , \quad (4)$$

where the external forcing f relates to the photospheric motions through $f = (v_A/L)\Psi$. This forcing can also be interpreted as an electric field generated by an electrostatic potential difference between the two photospheric plates ($z = 0$ and $z = L$). We choose a forcing term that is narrowband in wavenumber space and stationary in time, as described in the next section. A comparable approach was used by Einaudi et al. (1996), although with slight differences in the forcing term (see also Georgoulis, Velli, & Einaudi 1998).

3. DESCRIPTION OF THE SIMULATIONS

We performed numerical simulations of equations (3)–(4) on a square box of size $2\pi \times 2\pi$, assuming periodic boundary conditions. The magnetic vector potential and the stream function are expanded in Fourier series. To be able to perform long-time integrations, we worked with a moderate-resolution version of the code, with 192×192 grid points (in Dmitruk & Gómez 1997, we presented preliminary results with 96×96 resolution). The code is of a pseudospectral type, with 2/3 dealiasing (Canuto et al. 1988). The spectral equations for the time evolution of the system are:

$$\partial_t a_k = [\psi, a]_k - \eta k^2 a_k + f_k , \quad (5)$$

$$\partial_t w_k = [\psi, w]_k - [a, j]_k - \nu k^2 w_k . \quad (6)$$

For the nonlinear terms, we first compute the spatial derivatives in k-space. Next, we perform inverse FFTs and obtain the products required for the Poisson brackets in real space. Finally, we perform direct FFTs to obtain the Poisson brackets in k-space. To eliminate the aliasing in the transform operations, we make zero the Fourier components of modes with $k > N/3$, where N is the number of grid points in each direction. The temporal integration scheme is a fifth-order predictor/corrector, in order to achieve an almost exact energy balance over our extended time simulations (about 250 turnover times).

We model the external forcing in equation (5) as

$$f_k = \begin{cases} f_0 & \text{if } 3 < kl < 4 , \\ 0 & \text{elsewhere} , \end{cases} \quad (7)$$

with $f_0 =$ constant, to simulate the action of photospheric granular motions on the loop field lines. We chose a narrowband and nonrandom forcing to ensure that the broadband energy spectra and the signatures of intermittency that we obtained (see below) are exclusively determined by the nonlinear nature of the MHD equations.

We turn equations (3)–(4) into a dimensionless version, choosing l and L as the units for transverse and longitudinal distances, respectively. We choose $v_0 = f_0^{1/2}$ as the unit for velocities, since the field intensities are determined by the forcing strength. Since $f_0 = v_A \Psi/L$ and $v_{ph} = \Psi/l$, we have $f_0 = v_A v_{ph}(l/L)$, where v_{ph} is a typical photospheric velocity. The dimensionless dissipation coefficients are $\nu_0 = \nu/(l f_0^{1/2})$ and $\eta_0 = \eta/(l f_0^{1/2})$.

4. ENERGY DISSIPATION RATE

To restore the dimensions to our numerical results, we used typical values for the solar corona: $L \sim 5 \times 10^9$ cm, $l \sim 10^8$ cm, $v_{ph} \sim 10^5$ cm s^{-1}, $B_0 \sim 100$ G, and $n \sim 5 \times 10^9$ cm^{-3}. In addition, the values for the dissipation coefficients allowed by our moderate-resolution code are $\nu_0 = \eta_0 = 7 \times 10^{-3}$.

Figure 1 shows magnetic and kinetic energy versus time. After about five photospheric turnover times ($\tau_{ph} = l/v_{ph} \simeq 10^3$ s), a statistically steady state is reached. The behavior of both time series is highly intermittent despite the fact that the forcing is constant and coherent. Intermittent signals display activity during only a fraction of the time, which decreases with the scale under consideration. To quantify the degree of intermittency in a time series $S(t)$ (where $S(t)$ can be any relevant physical quantity, such as the magnetic or kinetic energy or the dissipation rate), we adopt the method described by Frisch (1996). We compute a high-pass filtered version of $S(t)$,

$$S_{w_c(t)} = \int_{|w| > w_c} dw e^{iwt} \hat{S}_w , \quad (8)$$

where $\hat{S}_w$ is the Fourier transform of $S(t)$ and w_c is the filter frequency. The flatness of the filtered signal is defined as

$$F(w_c) = \frac{\langle S_{w_c}^4(t) \rangle}{\langle S_{w_c}^2(t) \rangle^2} . \quad (9)$$

The characteristic feature of intermittent signals is that their associated flatness (as defined in eq. [9]) grows without bound with the filter frequency. This is indeed the case for our time series of total energy and dissipation rates, up to the numerical resolution of the filter frequency. The flatness $F(w_c)$ is a measure of the departure from Gaussianity of the signal $S(t)$ [$F(w_c) =$ const. $= 3$ for a Gaussian signal, since the filtering process is a linear operation, which therefore does not alter its Gaussian character].

This kind of behavior is usually called internal intermittency, to emphasize the fact that the rapid fluctuations

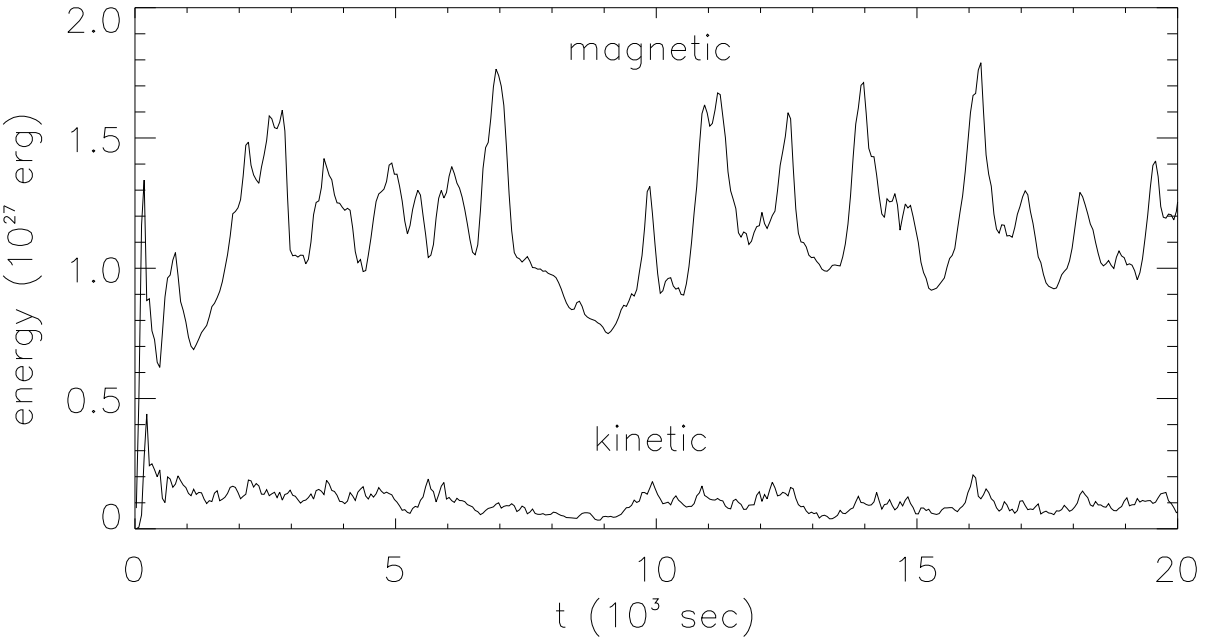

FIG. 1.—Total magnetic and kinetic energies as functions of time. Only the first 10% of the simulation is displayed, to show the details of these time series.

are not induced by an external random forcing. The forcing used by Georgoulis et al. (1998) also displays a slow time variation, but they introduced randomness in space by changing the places of the forcing vortices. Notwithstanding, many of their results are qualitatively consistent with the ones presented here, since spatial randomness is not an essential feature for the behavior of the average quantities.

Figure 1 also shows that the kinetic energy always remains at a small fraction of the magnetic energy in the stationary regime.

The energy dissipation rate is also a strongly intermittent quantity, as shown in Figure 2. For turbulent systems at large Reynolds numbers, the dissipation rate in the stationary regime is expected to be independent of the Reynolds number Re (Kolmogorov 1941). For the rather moderate Reynolds number simulations reported here, a weak (monotonically increasing) dependence of the dissipation rate with Re can be expected (see also Einaudi et al. 1996). However, comparing our results for a 96×96 resolution with those presented here (192×192), the increase in the heating rate is rather small (see Dmitruk & Gómez 1997). In addition, the dissipation rate is not completely independent of the spatial dependence of the forcing term. For instance, in our simulation only Fourier modes satisfying the ring condition $3 < kl < 4$ are externally driven. If we also drive the modes $\boldsymbol{k} = l^{-1}(\pm 3, 0)$, $\boldsymbol{k} = l^{-1}(\pm 4, 0)$, $\boldsymbol{k} = l^{-1}(0, \pm 3)$,

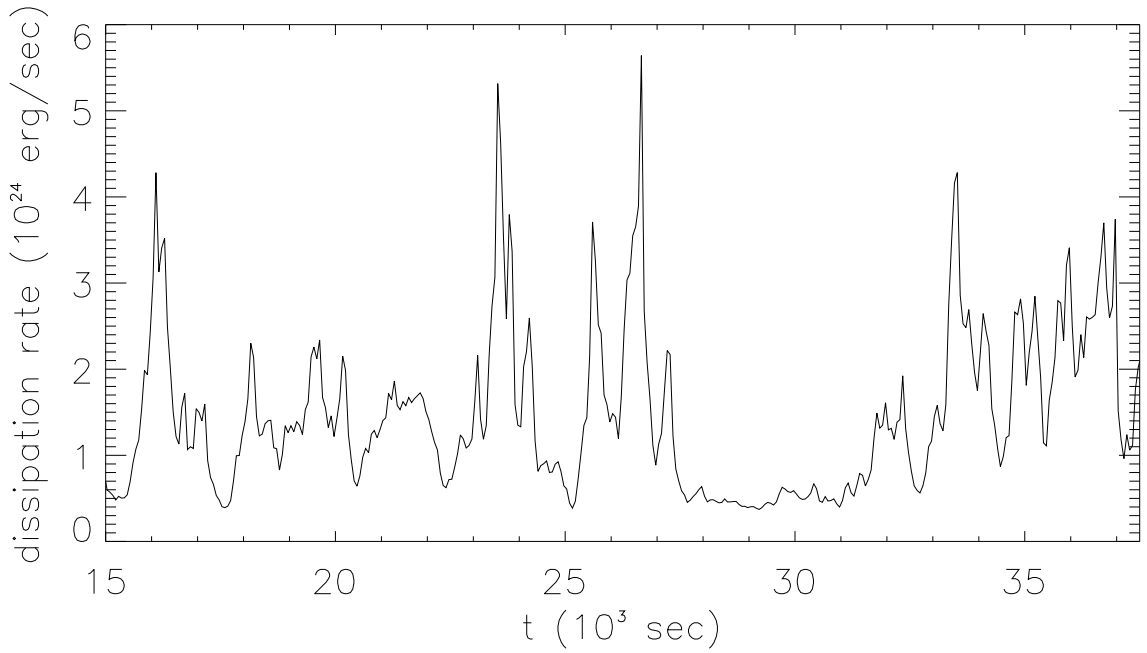

FIG. 2.—Time evolution of the energy dissipation rate. The interval from $t = 15 \times 10^3$ s to $t = 37 \times 10^3$ s is displayed, corresponding to the stationary regime.

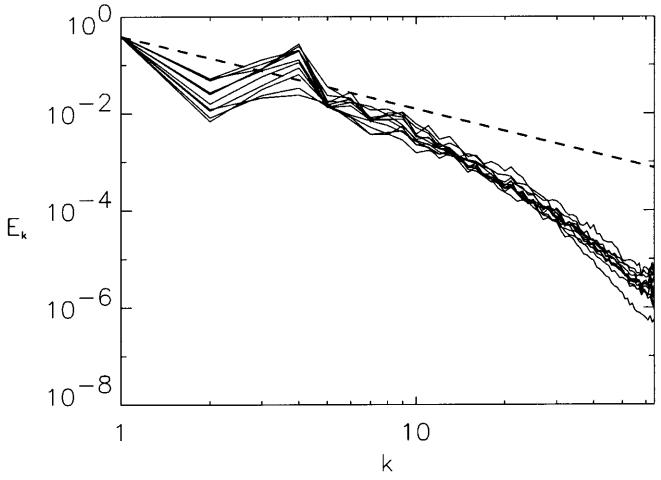

FIG. 3a

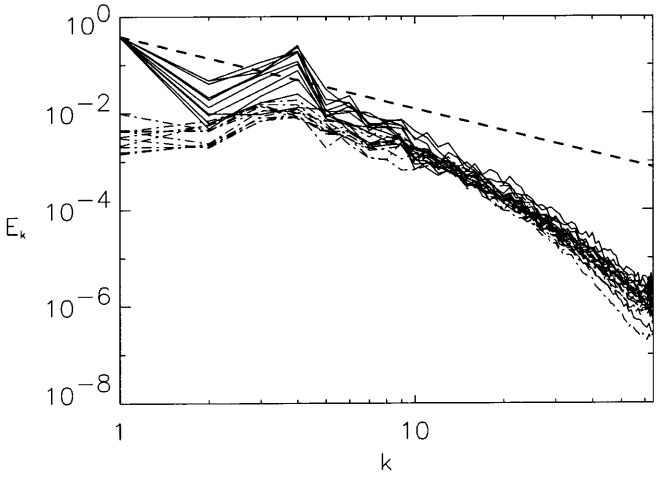

FIG. 3b

FIG. 3.—Energy spectra at ten different times (separated by $\Delta t = 50$ s) in the stationary turbulent regime. (*a*) Total energy; (*b*) magnetic (*solid lines*) and kinetic (*dot-dashed lines*) energies. The dashed line correspond to a Kraichnan spectrum, $E_k \sim k^{-3/2}$.

and $\boldsymbol{k} = l^{-1}(0, \pm 4)$, lying at the border of the ring, then the dissipation rate is larger and the behavior of the time series seems less intermittent. Since these modes correspond to purely one-dimensional spatial patterns, thus departing from the assumed isotropy for the photospheric velocity field, we exclude them from the forcing.

The total dissipation rate is given by

$$\epsilon \simeq 1.7 \times 10^{24} \text{ ergs s}^{-1} \left(\frac{B_0}{100 \text{ G}}\right)^{3/2} \left(\frac{v_{\rm ph}}{10^5 \text{ cm s}^{-1}}\right)^{3/2} \times \left(\frac{l}{10^8 \text{ cm}}\right)^{5/2} \left(\frac{n}{5 \times 10^9 \text{ cm}^{-3}}\right)^{1/4} \left(\frac{L}{5 \times 10^9 \text{ cm}}\right)^{-1/2}, \quad (10)$$

where we have also indicated the scaling with the relevant parameters of the problem. Using an Alfvén time $\tau_{\rm A} = L/v_{\rm A}$ and a photospheric time $\tau_{\rm ph} = l/v_{\rm ph}$, we can rewrite the dissipation rate as

$$\epsilon \sim B_0^2 v_{\rm ph}^2 l^2 L^{-1} \sqrt{\tau_{\rm A} \tau_{\rm ph}} . \quad (11)$$

The relevance of this functional dependence of the heating rate upon the physical and geometrical parameters of the system will be discussed in § 8.2.

We can transform the heating rate into an energy influx from the photosphere by simply dividing by twice the transverse area (because we have two boundaries), i.e., $\mathscr{F} = \epsilon / [2(2\pi l)^2]$. Note that the energy balance between the photospheric influx and Joule (and viscous) dissipation is a dynamic process. However, once the stationary turbulent regime is reached, the time averages of these energy rates (over timescales on the order of or larger than $\tau_{\rm ph}$, i.e., disregarding the intermittency structure) are equal.

Equation (12) shows the quantitative value of the energy influx as well as the explicit dependence with the relevant parameters of the problem,

$$\mathscr{F} = 2.1 \times 10^6 \text{ ergs cm}^{-2} \text{ s}^{-1} \left(\frac{n}{5 \times 10^9 \text{ cm}^{-3}}\right)^{1/4} \times \left(\frac{B_0}{100 \text{ G}}\right)^{3/2} \left(\frac{v_{\rm ph}}{10^5 \text{ cm s}^{-1}}\right)^{3/2} \left[\frac{l/(10^8 \text{ cm})}{L/(5 \times 10^9 \text{ cm})}\right]^{1/2} . \quad (12)$$

This energy flux compares quite favorably with the heating requirements for active regions, which span the range $\mathscr{F} = 3 \times 10^5$–$10^7$ ergs cm^{-2} s^{-1} (Withbroe & Noyes 1977).

From our simulations we can also obtain the "excess" velocity associated with the observed line broadening of a number of X-ray spectral lines in solar active regions (Seely et al. 1997; see also Saba & Strong 1991). We estimate this velocity as the root mean square value of the turbulent velocity field, which is proportional to the square root of the kinetic energy:

$$v_{\rm excess} = \left[\frac{2E^K}{n(2\pi l)^2 L}\right]^{1/2} . \quad (13)$$

The value from our simulation and the explicit dependence with the parameters of the problem is

$$v_{\rm excess} = 16 \text{ km s}^{-1} \left[\frac{B_0/(100 \text{ G})}{n/(5 \times 10^9 \text{ cm}^{-3})}\right]^{1/2} \times \left(\frac{v_{\rm ph}}{10^5 \text{ cm s}^{-1}}\right)^{1/2} \left[\frac{l/(10^8 \text{ cm})}{L/(5 \times 10^9 \text{ cm})}\right]^{1/2} . \quad (14)$$

This turbulent velocity is within the range of nonthermal line broadenings of ultraviolet spectral lines as measured by Cheng, Doschek, & Feldman (1979) (10–25 km s^{-1}) and from *SUMER* data by Seely et al. (1997) (22 km s^{-1}). These turbulent velocities, which presumably correspond to relatively cool and low-lying loops, are noticeably smaller than those derived from *SMM* data by Saba & Strong (1991) (50–60 km s^{-1}). The Saba & Strong (1991) turbulent velocities probably correspond to hotter and larger active regions, with a magnetic topology much richer than the one implied by the RMHD equations used for the present simulations. Also note that our heating rate (see eq. [12]) is still a factor of 5 smaller than the energy requirements for the hottest active regions. As discussed by Georgoulis et al. (1998), it is likely that in order to heat the largest active regions, full three-dimensional models are required.

5. ENERGY POWER SPECTRA

In spite of the narrow forcing and even though the velocity and magnetic fields are initially zero, nonlinear terms quickly populate all the modes across the spectrum. The total energy (magnetic plus kinetic) power spectrum is plotted in Figure 3*a*. The spectra correspond to different times in the stationary turbulent regime. The dashed line

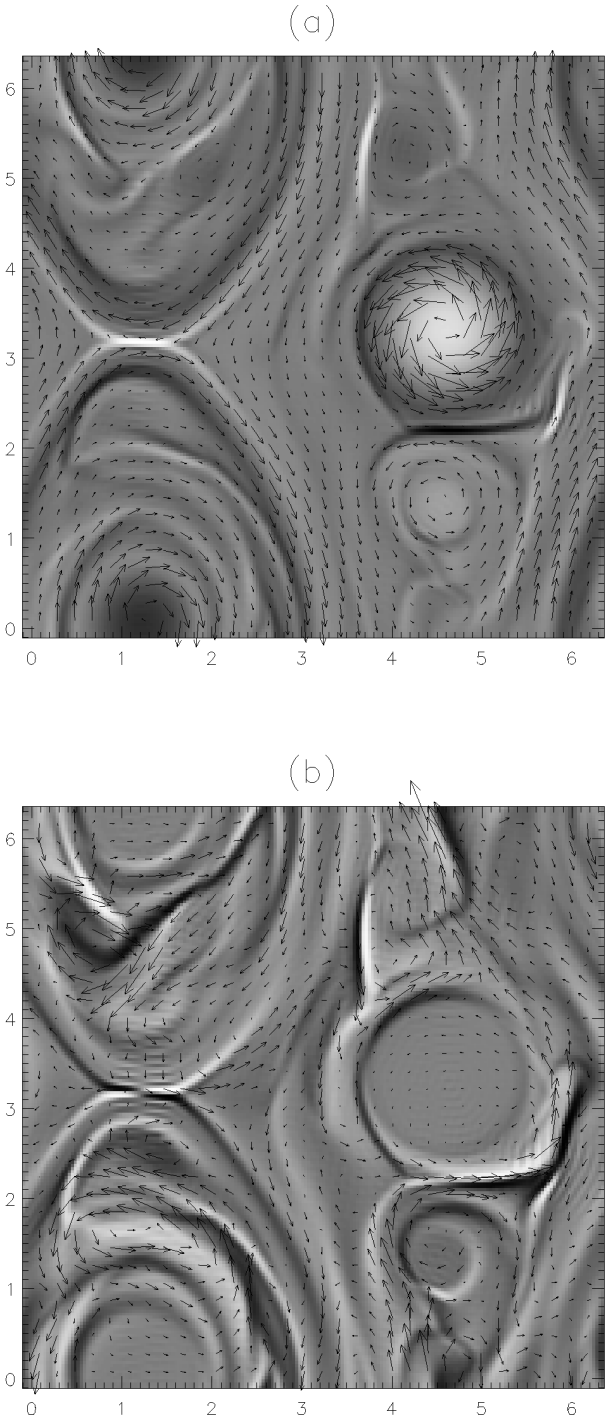

FIG. 4.—(*a*) Magnetic field arrows overlaid on a halftone of the electric current density at $t = 11 \times 10^3$ s. (*b*) Velocity field arrows overlaid on a halftone of vorticity.

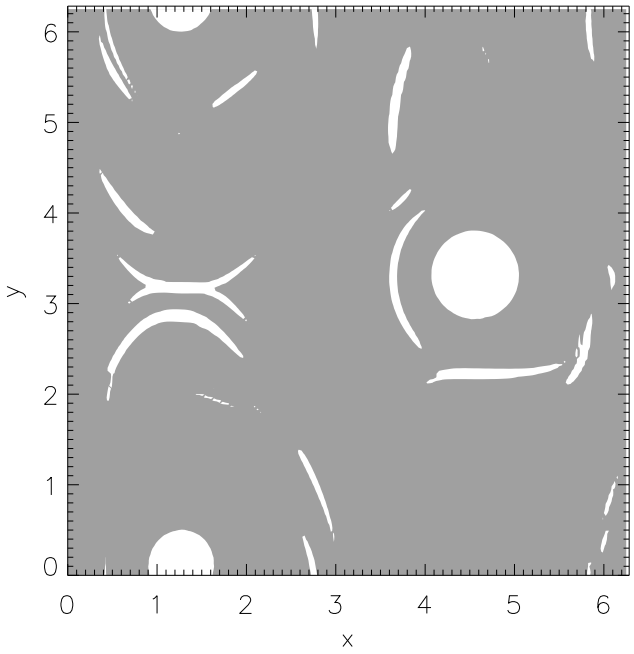

FIG. 5.—Zones of intense magnetic dissipation. White regions correspond to zones that concentrate 60% of the total dissipation, at time $t = 11 \times 10^3$ s.

corresponds to a Kraichnan spectrum ($E_k \sim k^{-3/2}$). In turbulent regimes, the effect of nonlinearities is to redistribute excitations in Fourier space in a virtually stochastic fashion. Since dissipative effects are only nonnegligible at very large wavenumbers, a net flow of excitations toward large wavenumbers is established to compensate for the dissipation. Energy is therefore injected into the system at low wavenumbers, cascades toward large wavenumbers in the so-called inertial range, and is efficiently quenched in the dissipative range. The Kraichnan spectrum is expected to be satisfied at the inertial range, where the role of external forcing and dissipation are negligible. For moderate-resolution simulations like the one presented here, the inertial range is rather limited, gradually entering into the dissipative range at $k > 10$, as shown in Figure 3.

In Figure 3*b* we plot the magnetic and kinetic spectra, showing that the spectra become close to equipartition ($E_k^M \sim E_k^K$) when approaching the dissipative range (large k). Nonetheless, note that the total kinetic energy (i.e., integrated over wavenumbers) remains much smaller than the total magnetic energy, as evidenced by Figure 1.

6. DISSIPATIVE STRUCTURES

Figure 4*a* shows the spatial distribution of electric current density for $t = 22\tau_{ph}$. Intense positive currents are shown by white regions, while intense negative current concentrations are indicated in black. The magnetic field is shown by arrows. This picture is a typical example of a strongly turbulent regime, with current concentrations of both O and X types. At the left center of the box there is a typical current sheet, of the type that result after the collapse of an X-type point. Moreover, the velocity field and vorticity displayed in Figure 4*b* confirm the standard picture of magnetic reconnection in current sheets, with Alfvénic jets emerging at the sides of the sheet and a quadrupolar distribution of vorticity. At the same time, Figures 4*a* and 4*b* show that in turbulent regimes there is also a rich variety of dissipative structure of different morphologies and degrees of complexity, in addition to the highly symmetric current sheet that we have just described. Figure 5 shows the spatial distribution and morphology of the most intense dissipative structures. The dissipation rate inside these structures is 60% of the total, although the filling factor is only 6%. This highly inhomogeneous distribution of energy dissipation is a manifestation of the spatial intermittency that is characteristic of turbulent regimes.

The thickness of current sheets is determined by the magnetic Reynolds number. In numerical simulations of turbulent regimes, the Reynolds number is usually made as large as possible, so that the sheet thickness (which is the smallest feature expected in these simulations) is just marginally resolved. The widths of these current sheets, on the other hand, are determined by the dynamics, and therefore a broad distribution of widths can be observed.

7. DISTRIBUTION OF EVENTS

Parker (1988) proposed that the energy dissipation of the stressed magnetic structures takes place in a large number of small events, which he termed "nanoflares." The superposition of a large number of such events would give the global appearance of a spatially homogeneous and stationary heating process. From a turbulent scenario, it seems quite natural to relate this spiky (both in space and time) heating to the internal intermittency present in all turbulent regimes.

We therefore associate the peaks of energy dissipation displayed in Figure 2 with the so-called nanoflares. We estimate the occurrence rate for these nanoevents, i.e., the number of events per unit energy and time $P(E) = dN/dE$, so that

$$\mathscr{R} = \int_{E_{\min}}^{E_{\max}} dEP(E) \tag{15}$$

is the total number of events per unit time and

$$\epsilon = \int_{E_{\min}}^{E_{\max}} dEEP(E) \tag{16}$$

is the total heating rate (in ergs s^{-1}) contributed by all events in the energy range $[E_{\min}; E_{\max}]$. A simple inspection of the $\epsilon(t)$ time series shown in Figure 2 indicates that these events are in a highly concentrated or piled-up regime, i.e., that their event rate $\mathscr{R}$ multiplied by their typical duration is much larger than unity. In this regime, many dissipation events are going off simultaneously at any given time. It is therefore impossible to perform a statistics of events, since we are unable to separate them.

As a way out to this difficulty, we define an event in the following fashion: first we set a threshold heating rate ϵ_0 on the time series displayed in Figure 2, on the order of its time average; "events" are then excesses of dissipation that start when $\epsilon(t)$ surpasses ϵ_0 and finish when $\epsilon(t)$ returns below ϵ_0. Once a particular threshold is set, we perform a statistical analysis of the events, keeping track of their peak values, durations, and total energy content. The implicit assumption behind our working definition is that the small fraction of events that emerge over the threshold are statistically representative of the whole set.

The occurrence rate as a function of energy (see Fig. 6*a*) displays a power-law behavior,

$$P(E) = AE^{-1.5\pm0.2}, \tag{17}$$

in the energy range spanning $E_{\min} \simeq 10^{25}$ ergs to $E_{\max} \simeq 2 \times 10^{26}$ ergs.

We also computed the distribution of events as a function of peak fluxes, which is a power law with slope $\alpha_P = 1.7 \pm 0.3$, as shown in Figure 6*b*. The slope we obtained is consistent with the one derived by Crosby, Aschwanden, & Dennis (1993) (1.68) from X-ray events and somewhat flatter than those reported by Hudson (1991) (1.8). The distribution of events as a function of their duration is shown in Figure 6*c*, displaying a slope of $\alpha_\tau = 1.9 \pm 0.2$.

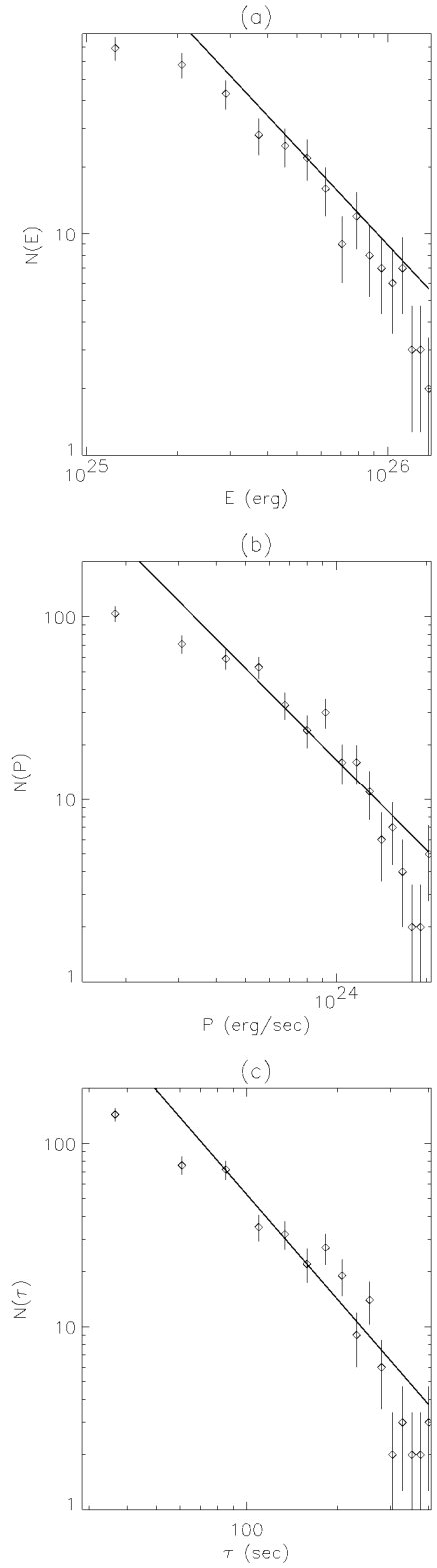

FIG. 6.—Occurrence rates of events as a function of (*a*) their energy, (*b*) their peak dissipation rate, and (*c*) their duration. Error bars indicate the statistical errors (square root of the number of counts) in each bin.

The error in the power-law indexes involve both the statistical error in each bin (see error bars in Fig. 6) and the error corresponding to the best fit to the data. The error

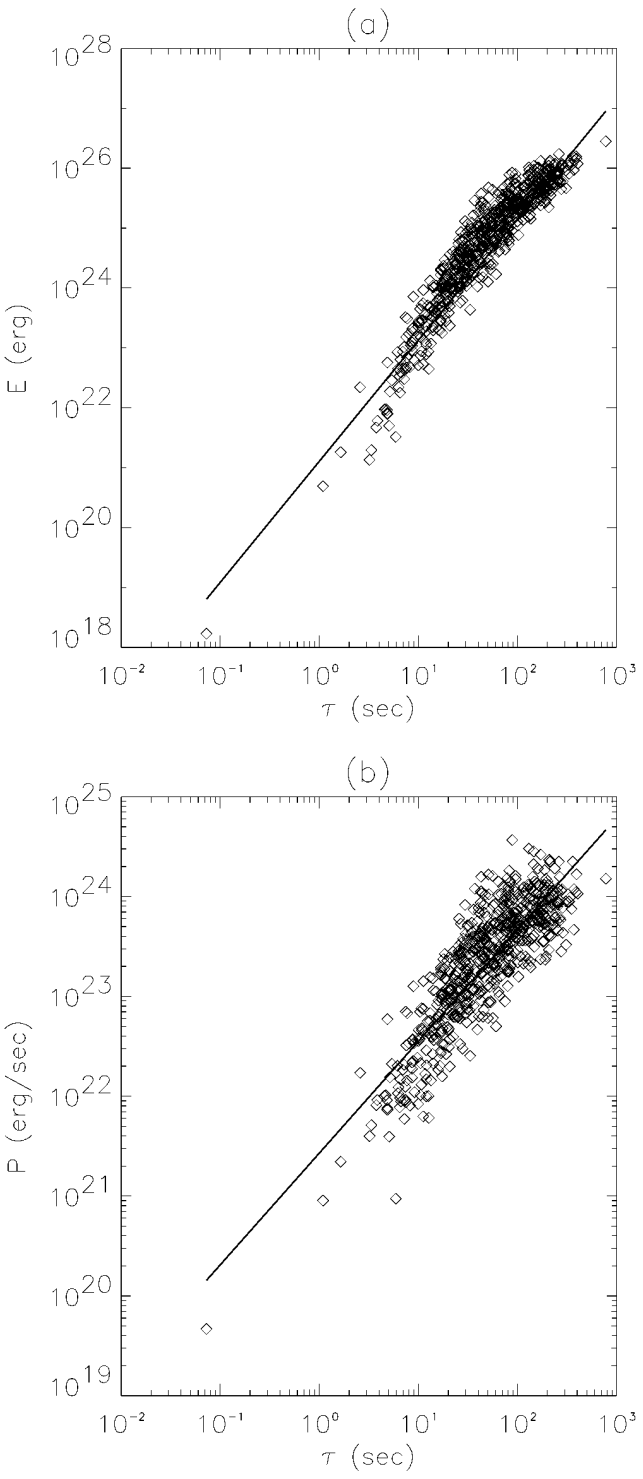

FIG. 7.—Correlations between parameters of events: (*a*) energy vs. duration; (*b*) duration vs. peak dissipation rate.

arising from different choices for the threshold ϵ_0 (which varies within a range such that the total number of events is maximum) is always smaller than the error sources mentioned above. A more technical procedure for choosing a threshold, which introduces a fitted χ^2 distribution to eliminate the noise, has been used in Georgoulis et al. (1998). This fitted threshold is slightly higher than the average value of the series.

Other important results from this statistical analysis are the correlations between the different parameters of these events. In Figure 7*a* there is a scatter plot of energy released versus event duration. The data can be fitted by a power law $E \sim \tau^{\gamma_{E\tau}}$, where $\gamma_{E\tau} = 2.02 \pm 0.02$. This result is consistent with the correlation reported by Lee, Petrosian, & McTiernan (1993) from hard X-ray observations. The duration versus peak correlation is plotted in Figure 7*b*, which can be fitted by $\tau \sim P^{\gamma_{\tau P}}$, where $\gamma_{\tau P} = 1.12 \pm 0.03$. These two correlation indexes agree with the approximate relationship

$$\gamma_{\tau P} \sim \gamma_{E\tau} - 1 , \tag{18}$$

which should be exact if the dimensional relationship $E \sim \tau P$ holds. Moreover, if these correlations are significant, then the different power-law indexes (α_E, α_P, and α_τ) should be mutually related through

$$\alpha_\tau = \gamma_{E\tau}\alpha_E - \gamma_{E\tau} + 1 , \tag{19}$$

$$\alpha_P = \frac{\gamma_{E\tau}\alpha_E - 1}{\gamma_{E\tau} - 1} . \tag{20}$$

Using $\alpha_E = 1.5$ and $\gamma_{E\tau} \simeq 2$ in equation (19), we obtain $\alpha_\tau \simeq 2$, in good agreement with the observed value of $\alpha_\tau = 1.9 \pm 0.2$. In addition, the predicted value for α_P from equation (20) is $\alpha_P \simeq 2$, which approximately agrees with the observed value of $\alpha_P = 1.7 \pm 0.3$.

8. DISCUSSION

8.1. *A Simple Model for Turbulent Dissipation*

In this section we summarize the main ideas of a model for turbulent dissipation that is an extension of the one sketched in Biskamp & Welter (1989) for decaying two-dimensional MHD turbulence. A detailed version can be found in Dmitruk & Gómez (1998).

We make the simplifying assumption that all the energy dissipation takes place inside current sheets of variable width λ and fixed thickness l_d, which is the dissipation length scale for this turbulent regime. The current sheets are formed between vortices of size λ, and therefore their width is also λ, which we assume as a free variable in order to perform a statistical analysis of dissipation events. We also assume that the energy spectrum follows a Kraichnan power spectrum, i.e., (see, e.g., Biskamp & Welter 1989)

$$E(k) = (\epsilon v_A)^{1/2} k^{-3/2} , \tag{21}$$

where ϵ is the dissipation rate and v_A^2 is the total magnetic energy per unit of mass,

$$v_A^2 = \int_{1/L_\perp}^{1/l_d} dk E(k) \simeq (\epsilon L_\perp)^{2/3} \tag{22}$$

and

$$L_\perp = 2\pi l,\ l_d = \left(\frac{\eta^2 v_A}{\epsilon}\right)^{1/3} = L_\perp R^{-2/3} , \tag{23}$$

where $R = (v_A L_\perp)/\eta$. From this spectrum, we can obtain a typical field (in units of velocity) in a vortex of size λ as

$$b_\lambda^2 = \int_{1/\lambda}^{1/l_d} dk E(k) \simeq (\epsilon v_A \lambda)^{1/2} , \tag{24}$$

so this is the typical field at the sides of a current sheet of width λ. In the present model, we assume a hierarchy of dissipative structures labeled by their values of λ, which are spatially distributed in such a way that their average

separation is also on the order of λ. The dissipation rate contributed by all the structures of width λ is therefore given by

$$\epsilon_\lambda = \frac{l_d \lambda}{\lambda^2} \eta \left(\frac{b_\lambda}{l_d}\right)^2 = \frac{\epsilon}{R^{1/3}} \left(\frac{\lambda}{L_\perp}\right)^{-1/2}, \quad (25)$$

since $(l_d \lambda/\lambda^2)$ is the area filling factor of current sheets of width λ, and the current density is approximately $j_\lambda \sim b_\lambda/l_d$.

The lifetime of these current sheets is determined by the nonlinear timescale in which the vortices of size λ break down and transfer their energy to smaller vortices as part of the turbulent cascade. This timescale is much shorter than the dissipation time of the current sheets, thus implying that two interacting vortices break down long before their energy is fully dissipated in the current sheet formed in between. The nonlinear timescale, following the Kraichnan model of MHD turbulence, is

$$\tau_\lambda = \frac{\lambda}{b_\lambda} \frac{\lambda/b_\lambda}{\lambda/v_A} = \frac{v_A^2}{\epsilon} \left(\frac{\lambda}{L_\perp}\right)^{1/2}. \quad (26)$$

In this stationary turbulent regime, the number of ongoing dissipation events of width λ per unit time is

$$N_\lambda = \left(\frac{L_\perp}{\lambda}\right)^2 \frac{1}{\tau_\lambda} = \frac{\epsilon}{v_A^2} \left(\frac{\lambda}{L_\perp}\right)^{-5/2}. \quad (27)$$

The energy dissipated in a single structure (current sheet) of size λ is then

$$E_\lambda = \frac{\epsilon_\lambda}{N_\lambda} = \frac{v_A^2}{R^{1/3}} \left(\frac{\lambda}{L}\right)^2. \quad (28)$$

Combining equations (27) and (28), we derive the distribution of events as

$$P(E) = \frac{dN_\lambda}{dE_\lambda} = \frac{\epsilon R^{1/3}}{v_A^4} \left(\frac{R^{1/3} E}{v_A^2}\right)^{-9/4} \sim E^{-\alpha_E}, \quad (29)$$

where $\alpha_E = 9/4 = 2.25$, which readily satisfies

$$\epsilon = \int_{E_{\min}}^{E_{\max}} dE E P(E), \quad (30)$$

where $E_{\min} = E_{\lambda = l_d} = v_A^2/R^{5/3}$ and $E_{\max} = E_{\lambda = L} = v_A^2/R^{1/3}$.

Therefore, according to this very simple model, the slope of the distribution of events is larger than 2, implying that small events dominate the heating process. There are several possible causes for this disagreement with the slope obtained from our simulation. (1) The theoretical model assumes that all the energy dissipation takes place in sheet structures formed by the coalescence of two vortices. Although our simulation shows that a fair fraction of the energy dissipation takes place in such structures, it is also clear that other structures, such as O-points, also contribute to the dissipation. (2) We assume that all current sheets have thickness l_d, which is likely to be an oversimplification. Depending on the parameters and boundary conditions under which current sheets are formed, different regimes of magnetic reconnection might occur, corresponding to different thicknesses. (3) To associate the lifetime of current sheets with the nonlinear timescale is also a simplification, since other processes might contribute to disrupt the current sheets once they are formed. (4) It might also be that our simulations with modest spatial resolution do not reflect the statistical properties of dissipative structures in a large Reynolds number regime. In addition, because of the characteristics of the simulations presented here, the current sheets are resolved only marginally. Simulations with higher resolution might provide a better understanding of the dynamics of these current sheets, which in turn will help to generate a more complete theoretical model.

From equations (28) and (26), the correlation between duration and dissipated energy becomes

$$E = \frac{v_A^2}{R^{1/3}} \left(\frac{\epsilon \tau_\lambda}{v_A^2}\right)^4 \sim \tau^{\gamma_{E\tau}}, \quad (31)$$

where $\gamma_{E\tau} = 4$.

The total event rate is then

$$\mathcal{R} = \int_{E_{\min}}^{E_{\max}} dE P(E) = \frac{\epsilon R^{5/3}}{v_A^2}. \quad (32)$$

To evaluate whether we are in a pile-up regime of dissipation events, we can compare the total event rate $\mathcal{R}$ with the shortest duration events (from eq. [26]):

$$\tau_{\lambda = l_d} = \frac{v_A^2}{\epsilon} \left(\frac{l_d}{L}\right)^{1/2} = \frac{v_A^2}{\epsilon} R^{-1/3}. \quad (33)$$

We obtain

$$\mathcal{R} \tau_{l_d} = R^{4/3} \gg 1. \quad (34)$$

Therefore, in a fully turbulent regime, the corresponding dissipation events always pile up.

In summary, from this rather simple model we can derive the following results: (1) a slope for the distribution of events, $\alpha_E = 2.25$ (see eq. [29]); (2) a power-law relationship between total dissipated energy and duration, $\gamma_{E\tau} = 4$ (see eq. [31]); and (3) a strong pile-up scenario for dissipation events.

8.2. *Heating Rate and Scaling Laws*

It is interesting to compare the heating rate scaling shown in equation (11) (§ 4) with the one arising from Parker's model (Parker 1972), in which the energy dissipated is assumed to match the energy injected by photospheric motions. When a field line is tilted by slow motions at its footpoints, a small transverse magnetic field component $\boldsymbol{b}$ is generated. The small tilt angle for a given field line after an elapsed time τ is b/B_0, which is in turn of the order of $v_{\rm ph} \tau/L$. Therefore, $b \simeq B_0 v_{\rm ph} \tau/L$. Assuming that the energy accumulated over the time τ completely dissipates, we obtain

$$\epsilon \sim \frac{L l^2 b^2}{\tau} = \frac{B_0^2 v_{\rm ph}^2 l^2}{L} \tau. \quad (35)$$

According to Parker (1983), footpoint motions pump energy into the coronal magnetic field until the angle between adjacent field lines reaches a critical value α_*. At this point, the built-up energy is suddenly released. Therefore, since $\alpha_* = v_{\rm ph} \tau/L$, the heating rate per unit volume scales as

$$H = \frac{\epsilon}{l^2 L} \sim \frac{B_0^2 v_{\rm ph}}{L} \alpha_*. \quad (36)$$

From our equation (11) (§ 4), it emerges that τ is an average between the Alfvén and photospheric timescales [$\tau \simeq (\tau_A \tau_{ph})^{1/2}$]. It is interesting to note that the timescale $\tau \simeq (\tau_A \tau_{ph})^{1/2}$ is also the growth time for nonlinear instabilities in an RMHD system (Gómez, De Luca, & McClymont 1993), which are responsible for the energy transfer in k-space. Thus, the heating rate per unit volume, according to the present model, scales as

$$H = \frac{\epsilon}{l^2 L} \sim \frac{B_0^{3/2}}{L^{3/2}} v_{ph}^{3/2} l^{1/2} n^{1/4} . \quad (37)$$

The particular dependence of the heating rate of a loop on its magnetic field B_0 and its length L is important, since the heating rate in turn relates to the thermodynamic variables of the loop (such as pressure and temperature) through the so-called scaling laws (Rosner, Tucker, & Vaiana 1978). The scaling laws are derived assuming a static balance between a uniform heating rate, thermal conduction, and (optically thin) radiative losses. In addition, the gas pressure is assumed to be uniform along the loop, which is a good approximation for loops with heights smaller than 10^5 km. The relationships between the heating rate H of a loop of length L with the thermodynamic variables P (pressure) and T (temperature) can be quickly derived by assuming that heating, conductivity, and radiative losses are all comparable. Therefore,

$$H \sim \kappa_0 \frac{T^{7/2}}{L^2} \sim \left(\frac{P}{T}\right)^2 \Psi_0 T^{-b} , \quad (38)$$

where κ_0 is the Spitzer conductivity and $\Psi(T) \simeq \Psi_0 T^{-b}$ is a power-law fit for the function of radiative losses for temperatures ranging from 10^6 to 5×10^6 K. The power index is $b \simeq 3/2$ in Porter & Klimchuk (1995) ($b \simeq 0.5$ in Rosner et al. 1978 and $b \simeq 1$ in Craig, McClymont, & Underwood 1978). From Parker's scaling ($H \sim B_0^2/L$; see eq. [36]), we obtain

$$T \sim (PL)^{4/(11+2b)} \sim (B_0^2 L)^{2/7} , \quad (39)$$

while for our scaling $H \sim (B_0/L)^{3/2}(P/T)^{1/4}$ (see eq. [37]), we obtain

$$T \sim (PL)^{4/(11+2b)} \sim (B_0^6 L)^{4/(49-2b)} . \quad (40)$$

Furthermore, if we use the power-law relationship $T \sim L^{\xi}$ derived by Porter & Klimchuk (1995) from observations, we can infer a relationship

$$B_0 \sim L^{x} \quad (41)$$

from either equation (39) or equation (40). Since according to Porter & Klimchuk (1995) the 90% confidence interval for ξ is $-0.58 \leq \xi \leq 0.16$, the corresponding interval for the power index x is (assuming $b \simeq 3/2$ in eq. [40]) $-1.3 \leq x \leq 0.1$ (although the case $x > 0$ seems very unlikely). From Parker's scaling (eq. [39]), a similar result is obtained ($-1.5 \leq x \leq -0.2$). It would certainly be very interesting to study the correlation between magnetic intensity and loop length directly from observations, to compare these to the functional dependence given in equation (41).

8.3. *Flares and Nanoflares*

In Dmitruk & Gómez (1997), we compared our occurrence rate versus energy with the one derived by Shimizu (1995) for transient brightening events observed by SXT on *Hinotori* and with that derived by Crosby et al. (1993) from *SMM* data. Not only are the slopes of these power-law curves quite comparable (between -1.5 and -1.6), but their total occurrence rates are also consistent with a single power law ranging from 10^{25} to 10^{33} ergs.

This remarkable correspondence indicates the presence of a common physical process behind the dissipation events throughout this extended energy range. The interpretation of the dissipative corona as a system in a state of self-organized criticality (see Bak, Tang, & Wiesenfeld 1988) has been suggested by Lu & Hamilton (1991). Cellular automata simulations of flares performed by Lu & Hamilton (1991) yielded the same power-law behavior for the occurrence rate, with a slope of -1.4. Since in all cases the index of the power law remains smaller than 2, equation (16) implies that the contribution to energy dissipation in a given energy range [E_{min}; E_{max}] is dominated by the most energetic events (i.e., $E \simeq E_{max}$). According to this result, the relatively infrequent large-energy events contribute more to the heating rate than the much more numerous small-energy events. Therefore, we speculate that the heating rate of a given active region is to some extent determined by the magnetic topology of that region. However, it is important to note that this is just one of the two possible scenarios for coronal heating. Hudson (1991) pointed out that this regime (dominated by large events) would reverse if there were a turn-up of the slope to values larger than 2 toward the low-energy end. Mercier & Trottet (1997) recently reported indirect evidence for such a turn-up from type I starburst observations. Vlahos et al. (1995) presented cellular automata simulations with an anisotropic rule for the redistribution of the magnetic field, and reported an index of -3.5 for the peak flux distribution. The model presented in § 8.1, based on Kraichnan's theory for stationary MHD turbulence, also yields an index larger than 2. Therefore, it seems apparent that to elucidate whether large or small events are dominant, more observational and theoretical efforts are required.

9. CONCLUSIONS

In the present paper we simulate the dynamics of a transverse section of a solar coronal loop through an externally driven two-dimensional MHD code. The relevant results of this study are as follows.

1. For an external forcing that is narrowband in wavenumber, we find that the system becomes strongly turbulent, and after about five photospheric turnover times a stationary turbulent regime is reached.

2. The energy dissipation rate obtained for typical footpoint velocities is consistent with the power necessary to heat active region loops ($\mathscr{F} \simeq 2.1 \times 10^6$ ergs cm^{-2} s^{-1}).

3. The energy dissipation rate displays a highly intermittent behavior, which is a ubiquitous characteristic of turbulent systems. Temporal intermittency manifests in the form of discrete-like dissipation events in the time series of the total energy dissipation rate. Spatial intermittency is also apparent, since a large fraction of the dissipation at any given time takes place in a rather small fraction of the volume.

4. A statistical analysis of dissipation events performed on a long-term numerical simulation (about 250 turnover times, which is roughly 3 days in real time) shows a power-

law event rate, proceeding as $dn/dE \sim E^{-1.5}$, that is remarkably consistent with the statistics of flare occurrence derived from observations (Hudson 1991; Crosby et al. 1993; Lee et al. 1993; Shimizu 1995).

5. The peak energy release and duration of events also follow power-law distributions. Furthermore, all these quantities are mutually correlated by power-laws.

We would like to sincerely thank to our referee, Giorgio Einaudi, for his constructive comments, which contributed to improve an earlier version of this manuscript. We acknowledge financial support by the University of Buenos Aires (grant EX247), Fundación Antorchas, and NASA (grant NAGW-4644).

REFERENCES

Bak, P., Tang, C., & Wiesenfeld, K. 1988, Phys. Rev. A, 38, 364
Biskamp, D., & Welter, H. 1989, Phys. Fluids B, 1, 1964
Canuto, C., Hussaini, M. Y., Quarteroni, A., & Zang, T. A. 1988, Spectral Methods in Fluid Dynamics (New York: Springer)
Cheng, C., Doschek, G., & Feldman U. 1979, ApJ, 227, 1037
Craig, I., McClymont, A., & Underwood, J. 1978, A&A, 70, 1
Crosby, N. B., Aschwanden, M. J., & Dennis, B. R. 1993, Sol. Phys., 143, 275
Dmitruk, P., & Gómez, D. O. 1997, ApJ, 484, L83
———. 1998, in preparation
Einaudi, G., Velli, M., Politano, H., & Pouquet, A. 1996, ApJ, 457, L113
Frisch, U. 1996, Turbulence (Cambridge: Cambridge Univ. Press)
Georgoulis, M., Velli, M., & Einaudi, G. 1998, ApJ, 497, 957
Gómez, D. O., & Ferro Fontán, C. 1992, ApJ, 394, 662
Gómez, D. O., DeLuca, E. E., & McClymont, A. N. 1993, ApJ, 448, 954
Hendrix, D. L., & van Hoven, G. 1996, ApJ, 467, 887
Heyvaerts, J., & Priest, E. R. 1992, ApJ, 390, 297
Hudson, H. S. 1991, Sol. Phys., 133, 357
Kolmogorov, A. N. 1941, Dokl. Acad. Sci. URSS, 30, 301
Lee, T. T., Petrosian, V., & McTiernan, J. M. 1993, ApJ, 412, 401
Lu, E. T., & Hamilton, R. J. 1991, ApJ, 380, L89
Mercier, C., & Trottet, G. 1997, ApJ, 474, L65
Parker, E. N. 1972, ApJ, 174, 499
———. 1983, ApJ, 264, 642
———. 1988, ApJ, 330, 474
Porter, L. J., & Klimchuk, J. A. 1995, ApJ, 454, 499
Rosner, R., Tucker, W. H., & Vaiana, G. S. 1978, ApJ, 220, 643
Saba, J., & Strong, K. 1991, ApJ, 375, 789
Seely, J. F., et al. 1997, ApJ, 484, L87
Shimizu, T. 1995, PASJ, 47, 251
Strauss, H. 1976, Phys. Fluids, 19, 134
van Ballegooijen, A. A. 1986, ApJ, 311, 1001
Vlahos, H., Georgoulis, M., Kluiving, R., & Paschos, P. 1995, A&A, 299, 897
Withbroe, G. L., & Noyes, R. W. 1977, AR&A, 15, 363